Energy Bands and Bloch States in 1D Laser Cooling and Their Effects on the Velocity Distribution

M. Doery, M. Widmer, J. Bellanca, E. Vredenbregt, T. Bergeman, and H. Metcalf
Physics Department, State University of New York, Stony Brook, New York 11794-3800
(Received 26 August 1993; revised manuscript received 17 January 1994)

We describe calculations that predict and analyze distinctive features in the velocity distribution in 1D laser cooling for light shift potential well depths only a few times the recoil energy. These features can be interpreted in terms of populations of energy bands or even Bloch states in the periodic potential. They occur with a σ^+ standing wave, with and without a small B field, and for lin $\perp$ lin laser cooling. We have observed these features experimentally in a beam of metastable helium atoms cooled on the $2^3S_1 \leftrightarrow 2^3P_2$ transition, with velocity resolution ~ 0.3 recoil.

PACS numbers: 32.80.Pj, 42.50.Vk

Recent progress in laser cooling has produced atoms with mechanical energies less than the light shifts induced by the laser light [1,2]. This means atoms may be confined in the wells of the periodic light shift potential. At such low energies, the atomic de Broglie wavelength is comparable to the optical wavelength. Motion in these wells is thus quantized: The eigenstates of atomic motion show a band structure analogous to that of electrons moving in the periodic potential of a crystal. Since a theory of this band structure in laser cooling was developed [3], there has been a keen interest in studying its effects experimentally. Recently, the frequency intervals between energy bands have been investigated with a probe laser using four-wave mixing [4], through sidebands in the fluorescence [5], and through rf spectroscopy [6]. Up to now, however, there have been no observations of quantum effects in the velocity distribution, which is arguably closer to the focus of laser cooling.

Here we report measurements and calculations that, for the first time, do reveal quantum effects in the velocity distribution, $P(V)$, of cooled atoms by comparison of experimental data with quantum calculations. We find effects of slower cooling rates for atoms in energy bands within the wells of the periodic light shift potential, $U(x)$, and effects of population transfer between Bloch states within these bands. In the latter cases, we are effectively probing the velocity substructure of bands in the periodic potential. Observation of these features requires that (a) the velocity resolution be smaller than the recoil velocity V_R; (b) the laser-atom interaction time must be at least a few times longer than the optical pumping time; and (c) $U(x)$ must be shallow enough so that only a few bands occur below the tops of the potential hills and tunneling between wells becomes appreciable. Conditions (b) and (c) are met by the choice of laser intensity and detuning, while (a) is facilitated by cooling metastable He 2^3S atoms (He*) on the $2^3S_1 \leftrightarrow 2^3P_2$ transition. He* has a large recoil velocity $V_R \equiv \hbar k/M = 9.2$ cm/s due to its small mass M ($\lambda \equiv 2\pi/k = 1.083$ μm is the laser wavelength).

We discuss three cooling configurations where we have observed energy band or Bloch state transition effects. The first is a pure σ^+ laser standing wave driving the He* $J = 1 \rightarrow 2$ transition, which produces a dip in $P(V)$ near $V = 0$. The dip is caused by slower cooling rates for atoms in the wells of $U(x)$, resulting in a deficiency of atoms in bands within these wells. The second configuration is magnetically induced laser cooling (MILC) where a σ^+ standing wave and a magnetic field produce sub-Doppler cooling [7]. Transitions between Bloch states *within* the lowest energy band in the standing wave produce a peak in $P(V)$ at $V = 0$ with a width about equal to V_R. The third case occurs in polarization gradient cooling by counterpropagating laser beams of orthogonal linear polarization (lin $\perp$ lin or LPL) [8]. Here we find dispersionlike features in $P(V)$ near $V = \pm V_R$, caused by net population transfer from states just above the lowest band gap to states just below it.

The apparatus used in our studies is shown schematically in Fig. 1. He* atoms come from a discharge-excited nozzle source, cooled by liquid N_2. The measured longitudinal velocity distribution has an average $v = 1400$ m/s and a spread $\Delta v_{\rm rms} = 240$ m/s at our standard operating conditions. The on-axis source output is $\sim 5 \times 10^{13}$ He* atoms s^{-1} sr^{-1}, while the ratio of singlet to triplet metastables in the beam is < 0.02. About 1 cm downstream of the nozzle there is a conical skimmer, followed 25 cm further by a 30 μm $\times$ 7 mm slit that reduces the flux to 2×10^8 He* atoms s^{-1}.

Directly after this slit, the atoms interact with two counterpropagating laser beams of equal intensity. The beams have a nearly Gaussian profile with a waist radius

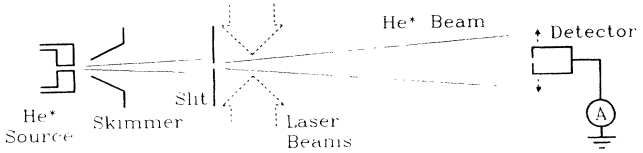

FIG. 1. Schematic of the experimental apparatus.

0031-9007/94/72(16)/2546(4)$06.00

TABLE I. Low order expressions for some unnormalized Mathieu functions, labeled by (n,ν) (adapted from Ref. [16]). Here $u = U_0/E_R$ and $z = kx$. Energies (third column) are relative to the potential mean.

(n,ν)	Ψ	E/E_R
0,0	$1-(u/8)\cos(2z)\ \ldots$	$-u^2/32\ \ldots$
0,0.8	$\exp(0.8iz)-(5u/16)\exp(-1.2iz)\ \ldots$	$0.64-0.09u^2\ \ldots$
0,1	$\sin(z)-(u/32)\sin(3z)\ \ldots$	$1-u/4\ \ldots$
1,1	$\cos(z)-(u/32)\cos(3z)\ \ldots$	$1+u/4\ \ldots$
1,0.8	$\exp(-1.2iz)+(5u/16)\exp(0.8iz)\ \ldots$	$1.44+0.07u^2\ \ldots$

$w = 16$ mm (e^{-2} intensity point) and are apertured to a diameter of 32 mm. They originate from a home-built, laser diode-pumped cw LNA laser [9]. The laser's frequency is locked to a cavity locked to a Zeeman-tuned [10], weak rf discharge in helium. The interaction region is surrounded by three orthogonal pairs of Helmholtz coils to create a well-defined magnetic field **B**. The Earth's magnetic field was canceled to ± 5 mG using the mechanical Hanle effect on the $2^3S_1 \rightarrow 2^3P_1$ transition [11].

The transverse $P(V)$ of the He* beam, modified by interaction with the laser light, is measured with a detector 1.9 m away. This detector consists of a stainless steel plate placed behind a 30 μm wide slit in a moveable, metal cage. The two 30 μm slits separated by 1.9 m provide velocity resolution of 2.7 cm/s or 0.3 V_R. The internal energy of the He* atoms can free an electron from the plate on impact, and the resulting current (~ 10 fA) is amplified, collected, and recorded. The detector's transverse position is scanned with a stepper motor.

We have used two types of density matrix quantum cooling calculations [3,12–14] to interpret the measurements. The density matrix ρ obeys the Liouville equation $\dot{\rho} = -(i/\hbar)[H,\rho] + \dot{\rho}_{\rm se}$, where H includes internal and kinetic energies and atom-laser and magnetic field interactions. $\dot{\rho}_{\rm se}$ expresses the spontaneous radiative decay and repopulation of ground state sublevels. The calculations that best model the experiments use basis states that are products of internal atomic states and free particle momentum eigenfunctions [3,13]: $\Psi = |J,m,p\rangle$. Excited states are explicitly included so Doppler cooling effects occur, and the laser profile can vary in space. These calculations match the measured $P(V)$, but alone they do not offer a clear picture of the cooling process.

More insight comes from using the eigenstates $\Psi(x)$ of $U(x)$, obtained by adiabatically eliminating the excited state [12,14,15]. It is sometimes useful to project free particle computational results onto the $\Psi(x)$. Also calculations directly with a density matrix over the $\Psi(x)$ represent the essential features for MILC and LPL cooling, although there is no Doppler cooling and the laser profile is assumed constant. In this method, the effective ground state Hamiltonian is $H_{\rm eff} = P^2/2M + (2S\delta/L)V_{ge}V_{eg}$, where $S \equiv 2\Omega^2/\Gamma^2$ ($= 1$ for intensity $I = \pi hc/3\lambda^3\tau$), Ω is the single beam Rabi frequency, $\Gamma \equiv 1/\tau$ is the decay rate, $\delta \equiv \omega_{\rm laser} - \omega_{\rm atom}$ is the laser detuning from the atomic frequency, and $L \equiv 1 + 4\delta^2/\Gamma^2$. The matrix V_{ge} includes Clebsch-Gordan coefficients for the atom-laser interaction ($|V_{gi,ej}| \leq 1$). $H_{\rm eff}$ is diagonal in the magnetic quantum number m for σ^+ light or for LPL cooling on a $J_g = \frac{1}{2}$ transition. As discussed in Ref. [3], the secular approximation (no off-diagonal density matrix elements) may normally be used for LPL. The well depth $U_0 = fS\delta/L$, where $f = 2$ for a σ^+ standing wave, and $f = 5/6$ for $J = 1 \rightarrow 2$ for LPL.

Some background on Bloch states is helpful. When $H_{\rm eff}$ is diagonal, the eigenfunctions satisfy a Mathieu equation. Solutions may be written as an expansion in momentum eigenstates [3,15,16] $\Psi_{n,\nu}(x) = \sum_j a_{n,j,\nu} \exp[i(\nu + 2j)kx]$, where n is the band number and ν is the Bloch index: $-1 < \nu \leq 1$. Thus $\Psi(x)$ obeys Floquet's theorem. Table I presents the low order wave functions for $U(x) = U_0 \sin^2(kx)$, when $U_0 < E_R = MV_R{}^2/2 = \hbar^2k^2/2M$, the recoil energy. Energy gaps occur at $\nu = 0$ or ± 1. When $U(x)$ is shallow, quasibound states ($E < U_0$) just below a gap are more strongly localized in the deep part of the wells than states just above it, but the $\nu = 0$ state of the lowest ($n = 0$) band is only slightly localized.

To explain our observations in the simplest way, we will refer to $J = \frac{1}{2} \rightarrow \frac{3}{2}$ models. For MILC and LPL, we use a basis of eigenstates of $H_{\rm eff}$ and assume that the atomic recoil from spontaneous emission of a π (σ) photon is always directed perpendicular (parallel) to the laser axis (x axis). In σ^+ excitation from $m = -\frac{1}{2}$ Bloch states, followed by π decay to $m = \frac{1}{2}$ states, the net change in the Bloch index is then $\Delta\nu = \pm 1$.

We first discuss a feature in σ^+ standing wave laser cooling (no polarization gradients or magnetic field). The data in Fig. 2(a) show an overall bell shape from the initial $P(V)$ modified by normal Doppler cooling. In addition, there is a dip near $V = 0$, which is reproduced in the computational results obtained with the free particle basis (with Gaussian laser spatial profile), shown with the solid line. The dashed line shows similar results calculated for a $J = 0 \rightarrow 1$ transition also with a σ^+ standing wave laser field, or effectively with 2-level Doppler cooling. This calculation also exhibits a dip at $V = 0$ of about the same amplitude but slightly different shape.

From the computational results in Fig. 2(a), we conclude that the major part of the observed dip at $V = 0$ is due to an effect discussed previously in semiclassical terms [17], but not yet reported in experimental observations of $P(V)$. Atoms with $E_{\rm kin} < U_0$ are cooled more slowly than those with higher $E_{\rm kin}$, thus accumulate more slowly than those with $E_{\rm kin} > U_0$. We show this in terms of the population of quantum levels in $U(x)$ by projecting the calculated density matrix over the free particle basis states onto eigenfunctions of $U(x)$. Figure 3(a) shows $m = \pm 1/2$ ground state energy bands for a $J = 1/2 \rightarrow 3/2$ transition, while Fig. 3(b) shows the populations in these bands, in each case for spatially uniform laser intensity after 20 μs. The $m = -1/2$ bands

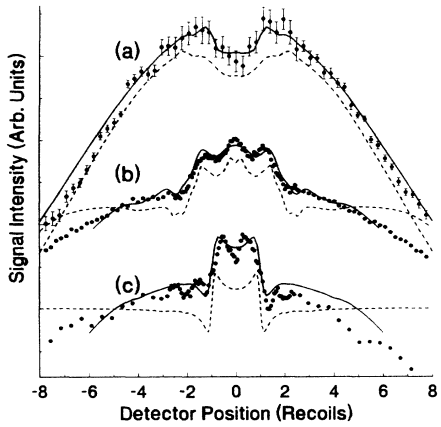

FIG. 2. Experimental data (dots) and free particle basis computational results (solid lines) for the velocity distribution of He^* atoms with (a) a σ^+ standing wave, $S_{max} = 1.65, \delta = -2\Gamma$; (b) a σ^+ standing wave plus 50 mG B field, $S_{max} = 4.5, \delta = -4\Gamma$; (c) LPL cooling, $S_{max} = 2.7, \delta = -8\Gamma$. For (c), calculations were performed with $S_{max} = 1.2$. The laser intensity has a Gaussian spatial distribution. The dashed line for (a), displaced for clarity, gives computational results for the identical conditions as for the solid line but for a $J = 0 \rightarrow 1$ rather than $J = 1 \rightarrow 2$ transition. Dashed lines for (b) and (c) give results of periodic potential basis calculations for the simpler case of $J = 1/2 \rightarrow 3/2$, with adjusted uniform laser intensity.

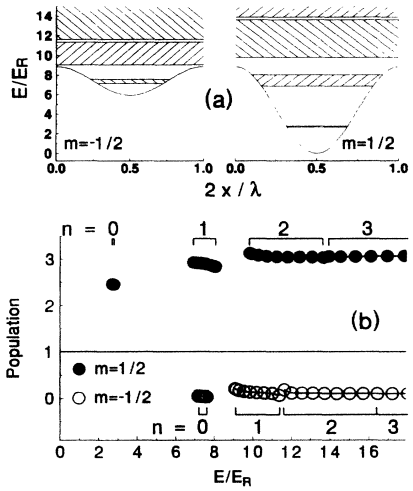

FIG. 3. Analysis of the quantum feature in Fig. 2(a), using computational results for a $J = 1/2 \rightarrow 3/2$ transition with a σ^+ standing wave, spatially uniform laser intensity, $S = 1$, and $\delta = -2\Gamma$ ($U_0/E_R = 8.9$). (a) Light shift potentials for $m = \pm 1/2$, with the lowest few energy bands. (b) Populations of Bloch states (discretized on a mesh of $\Delta\nu = 0.1$) in the lowest $m = \pm 1/2$ bands after 20 μs (200 τ), relative to the uniform initial population (solid line at 1). The braces (top and bottom) indicate the energy range of each band.

have been depopulated by optical pumping in the σ^+ light. The lowest $m = 1/2$ band (n=0) has fewer atoms than expected by extrapolation from bands lying above $E = U_0$. Hence there is a deficiency of atoms near $V = 0$ in this simplified model and a closely related dip at $V = 0$ in the experimental data.

At present, only fully quantum calculations reproduce the data quantitatively. Semiclassical Fokker-Planck methods using a spatially averaged force do not give a dip at $V = 0$. We find that calculations of trajectories with the semiclassical $F(X, V)$ force function [17,18] (with no diffusion) for an ensemble of values of X and V do yield a dip for certain laser parameters.

The difference between the $J = 0 \rightarrow 1$ and $J = 1 \rightarrow 2$ computational results in Fig. 2(a) is due to transfer from the lowest quantum states of $m = -1$ and 0 sublevels to $m = 1$. This momentum transfer process (MT) appears again in MILC (below). The dip at $V = 0$ is relatively short lived. For $m = 1$ atoms, Doppler cooling and equilibration with the laser field continue at the rate $\Gamma_{Dopp} = 16 S\delta E_R/\hbar\Gamma L^2$. Since our interaction time is only ~ 20 μs, we do not see the dip vanish, but our calculations indicate that it disappears after about 200 μs.

The next feature we discuss occurs when a transverse magnetic field B is added to the σ^+ standing wave (MILC [7]). At low intensities the two peaks from the MT process appear at approximately $\sim V = \pm 1.3 V_R$. As discussed in Ref. [13], MILC is a cyclic process of $\Delta m = +1$ optical pumping and $\Delta m = \pm 1$ B field mixing. Hence in MILC, the peaks at $V = \pm 1.3 V_R$ are continually regenerated. Also in Fig. 2(b) there is a central peak of width $\sim V_R$. As shown in Fig. 4(a), the population of the lowest $m = -1/2$ band decreases sharply with energy. No central peak occurs when the populations of the Bloch states in this band are artificially made uniform, as they nearly are for the $\mathbf{B} = 0$ case. We conclude that the variation in the population over the band is responsible for the peak in $P(V)$ at $V = 0$ in Fig. 2(b).

To show why this variation occurs, in Fig. 4(b) transitions between Bloch states (labeled A through D) in the lowest bands ($n = 0$) of the $m = \pm\frac{1}{2}$ potentials are represented by straight and curved (single) arrows. The numbers (0.87, etc.) give the relative pumping transition rates between states $|m, n, \nu\rangle$ as $T_{AD} = |\langle -\frac{1}{2}, 0, 0|\sin(kz)|\frac{1}{2}, 0, 1\rangle|^2 = 0.80$ and $T_{BC} = |\langle -\frac{1}{2}, 0, 1|\sin(kz)|\frac{1}{2}, 0, 0\rangle|^2 = 0.87$. In the deeper, $m = +\frac{1}{2}$ well, all states are comparably localized near the high intensity region, but in the shallow $m = -\frac{1}{2}$ well, the $n = 0$ wave functions become more strongly localized in the high-intensity part of the well as ν goes from 0 to 1. Therefore T_{BC} is greater than T_{AD}. The pumping rate from $m = -\frac{1}{2}$ to $m = \frac{1}{2}$ for $\nu = 0$ (point A) to $\nu = 1$ (D) is weaker than the pumping rate from $\nu = 1$ to $\nu = 0$ (B to C) because atoms at B experience a higher average intensity than those at A. By contrast, the $\mathbf{B}$ field mixing rate between the two $\nu = 1$ states (B, D) is very nearly equal to that for $\nu = 0$ (A, C). The net result of this cyclic process is an accumulation of atoms in the state with the lowest pumping rate, i.e., state A [double arrow in Fig. 4(b)]. As seen from Table I and Fig.

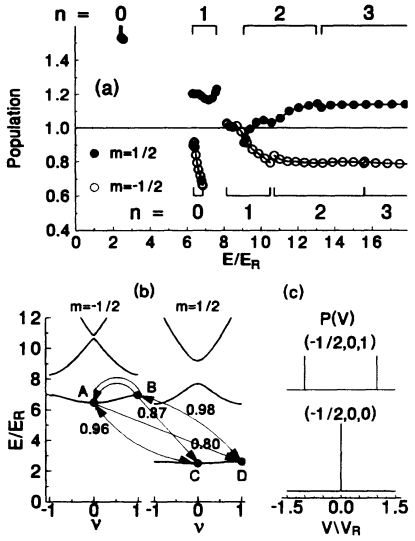

FIG. 4. Analysis of the quantum feature in Fig. 2(b) (MILC) based on calculations for a $J = 1/2 \rightarrow 3/2$ transition in a σ^+ standing wave, $S = 2$, $\delta = -5\Gamma$ ($U_0/E_R = 8.0$), $B = 50$ mG. (a) Calculated populations in Bloch states as in Fig. 3(b). (b) Low-lying energy bands vs Bloch index ν for $m = \pm 1/2$, with optical pumping (straight arrows) and B field coupling (curved single arrows) transition elements. The double arrow shows the net population transfer. (c) $P(V)$ functions for the $m = -1/2, n = 0, \nu = 0$, and $\nu = 1$ Bloch states, initial and final states of the two-step transfer process.

4(c), atoms with $\nu = 0$ have a large probability to be at $V = 0$. Thus, a central peak occurs because of a two-step transfer of atoms *within* the lowest $m = -\frac{1}{2}$ energy band, and is a purely quantum feature. For deeper potentials with more bands below the tops of the potential hills, this quantum feature evolves into the usual MILC cooling peak.

Our third feature, also a quantum effect, occurs in LPL polarization gradient cooling at low intensities. For $U_0 \sim E_R$, we find that $P(V)$ has strong dispersion shapes centered at $V = \pm V_R$, which can also be understood in terms of transitions between Bloch states within the low-lying energy bands. Calculations and experimental data on this effect are shown in Fig. 2(c). To best match the experimental data, a laser intensity $S = 1.2$ was used in the calculations as compared with the measured value of 2.7. This discrepancy is unexplained at present.

In LPL cooling, each optical pumping step of the cyclic transfer from $m = -\frac{1}{2}$ to $m = \frac{1}{2}$ and back results in some energy loss. With shallow potentials, the lowest quantum states produce anomalies in the cooling process. We focus on optical pumping or radiative decay from the $m = -\frac{1}{2}, n = 1$ band to the $m = \frac{1}{2}, n = 0$ band, and consider atoms in Bloch states labeled A, B, and C in Fig. 5. Atoms in Bloch state A are pumped to state B by σ^+ photons, then to C by σ^- photons (Fig. 5). The rate for this pumping into C is faster than the rate for pumping atoms out of C to higher states, so there is a net transfer of atoms from A to C. For A, the most probable

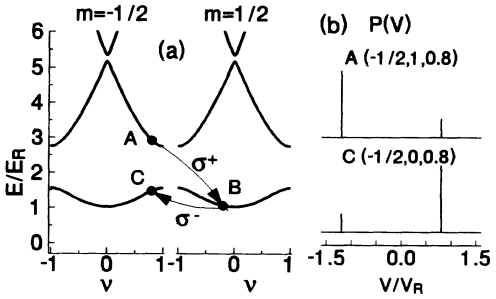

FIG. 5. Analysis of the quantum feature in LPL cooling in Fig 2(c), in terms of a $J = 1/2 \rightarrow 3/2$ transition. (a) Low-lying energy bands for $m = \pm 1/2$, with arrow showing important transitions between Bloch states. (b) $P(V)$ functions for the initial and final Bloch states in the two-step transfer in (a).

$|V|$ is slightly $> V_R$, while for C, the most probable $|V|$ is slightly $< V_R$, as seen from the $P(V)$ in Fig. 5(b) or the (1,0.8) and (0,0.8) functions in Table I. This two-step transition accounts for the dip at $V > V_R$ and the peak at $V \lesssim V_R$, and reflects the differing character of Bloch states just above and just below the lowest band gap.

In summary, the experiments and calculations reported here show that in order to understand laser cooling on the level of one recoil velocity, one must understand the redistribution of population among Bloch states in the periodic light shift potential.

This work was supported by NSF, ONR, AFOSR, the U.S. Department of Education, and by a grant of computer time from the Cornell National Supercomputer Facility.

[1] P. Lett *et al.*, Phys. Rev. Lett. **61**, 169 (1988).
[2] C. Salomon *et al.*, Europhys. Lett. **12**, 683 (1990).
[3] Y. Castin and J. Dalibard, Europhys. Lett. **14**, 761 (1991).
[4] P. Verkerk *et al.*, Phys. Rev. Lett. **68**, 3861 (1991) .
[5] P. Jessen *et al.*, Phys. Rev. Lett. **69**, 49 (1992).
[6] R. Gupta *et al.*, in *Proceedings of the International School of Physics "Enrico Fermi,"* Course CXVIII, edited by E. Arimondo and W. Phillips (North-Holland, Amsterdam, 1992), p. 345.
[7] B. Sheehy *et al.*, Phys. Rev. Lett. **64**, 858 (1990).
[8] J. Dalibard and C. Cohen-Tannoudji, J.Opt. Soc. Am. B **6**, 2023 (1989).
[9] T. Chuang and H. Metcalf, Appl. Opt. **30**, 2495 (1991).
[10] T. Dineen *et al.*, Opt. Commun. **92**, 277 (1992).
[11] R. Kaiser *et al.*, Z. Phys. D **18**, 17 (1991).
[12] Y. Castin, J. Dalibard, and C. Cohen-Tannoudji, in *Light Induced Kinetic Effects on Atoms, Ions and Molecules*, edited by L. Moi *et al.* (ETS Editrice, Pisa, 1991).
[13] T. Bergeman, Phys. Rev. A **48**, R3425 (1993).
[14] M. Doery, E. Vredenbregt, and T. Bergeman (to be published).
[15] M. Wilkens *et al.*, Phys. Rev. A **44**, 3130 (1991).
[16] N. MacLachlan, *Theory and Application of Mathieu Functions* (Dover, New York, 1964).
[17] N. Bigelow and M. Prentiss, Opt. Lett. **15**, 1479 (1990).
[18] J. Gordon and A. Ashkin, Phys. Rev. A **21**, 1606 (1980).